

Quantum subspace alignment for domain adaptation

Xi He^{1,*} and Xiaoting Wang^{1,†}

¹*Institute of Fundamental and Frontier Sciences,
University of Electronic Science and Technology of China*

Domain adaptation (DA) is used for adaptively obtaining labels of an unprocessed data set with given a related, but different labelled data set. Subspace alignment (SA), a representative DA algorithm, attempts to find a linear transformation to align the two different data sets. The classifier trained on the aligned labelled data set can be transferred to the unlabelled data set to classify the target labels. In this paper, a quantum version of the SA algorithm is proposed to implement the domain adaptation procedure on a quantum computer. Compared with the classical SA algorithm, the quantum algorithm presented in our work achieves at least quadratic speedup in the number of given samples and the data dimension. In addition, the kernel method is applied to the quantum SA algorithm to capture the nonlinear characteristics of the data sets.

I. INTRODUCTION

Transfer learning is a crucial subfield of machine learning and it aims to accomplish tasks on an unprocessed data set with the known information of a different, but related data set [1]. In the realm of transfer learning, domain adaptation (DA) specifically attempts to predict the labels of the unprocessed data set based on the given labelled data set and has been widely used in natural language processing and computer vision [2]. DA can be categorized as the semi-supervised DA and the unsupervised DA. The semi-supervised DA refers to a common method where the unprocessed data set has a few labels [3–6]. The unsupervised DA focuses on the task that the unprocessed data set is totally unlabelled [7–9]. As one of the most representative kind of unsupervised DA algorithms, subspace learning assumes that the data distributions of the labelled data set will be similar to the data distributions of the unlabelled data set after some transformations [2]. The subspace learning algorithm mainly contains two types including the statistical-based subspace learning [10–12] and the manifold-based subspace learning [13, 14] in the view of transformation modes. The former method mainly aligns the statistical features of the two data sets. The latter maps the original data to some manifold and transforms the labelled data to the target unlabelled data sequentially.

Subspace alignment (SA) is one of the most concise and efficient statistical-based subspace learning algorithms. After preprocessing the original data sets to eliminate the redundant information, we attempt to find a linear transformation matrix to align the subspace of the labelled data set to the subspace of the unlabelled data set. Subsequently, the classifier can be performed on the aligned subspace data to obtain the target labels. Compared with other domain adaptation algorithms, SA is efficient in domain adaptation and easy to implement. In addition, SA manipulates the global covariance ma-

trices and is intrinsically regularized [10]. However, with the increase of the scale of the data set and the dimension of the data points, the algorithmic complexity of the classical SA algorithm can be costly.

Compared with classical computation, quantum computation proposes a new computing pattern utilizing the principles of quantum mechanics [15–19]. It can be applied to the field of machine learning to achieve quantum speedup in computational complexity compared with the corresponding classical algorithms [20–22]. Concretely, for the shallow machine learning, quantum computing techniques can be applied to deal with supervised learning tasks such as classification [23–25], data fitting [26, 27] and unsupervised learning tasks including clustering [28] and dimensionality reduction [29, 30]. For the deep learning, the feedforward neural network [31] and the generative models such as quantum auto-encoders [32–34], quantum Boltzmann machine [35, 36] and quantum generative adversarial network [37–42] can be implemented on quantum devices. Recently quantum computation can be combined with transfer learning to promote the performance of hybrid classical-quantum neural networks [43]. In addition, the transfer component analysis algorithm can be implemented on a quantum computer with transforming the procedure of data distribution domain adaptation into solving the eigenproblem of a specified matrix [44].

In this paper, a quantum version of the classical SA algorithm is proposed. In the data preprocessing, we adopt the quantum principal component analysis (qPCA) to transform the given data sets from the original D -dimensional space to their d -dimensional subspaces in $O(d \log D)$ where $d \ll D$ [21]. Compared with the classical SA requiring runtime in $O(D^2 d)$, the quantum subspace alignment algorithm (qSA) can be implemented on a quantum computer in $O(\text{poly}(\sqrt{D}))$ achieving quadratic speedup [45]. In addition, the quantum nearest-neighbor algorithm [24, 25], a local classifier and the quantum support vector machine algorithm (qSVM) [23], a global classifier can be performed on the subspace data sets to classify the target labels with quadratic and exponential speedup respectively. There-

* xihe@std.uestc.edu.cn

† xiaoting@uestc.edu.cn

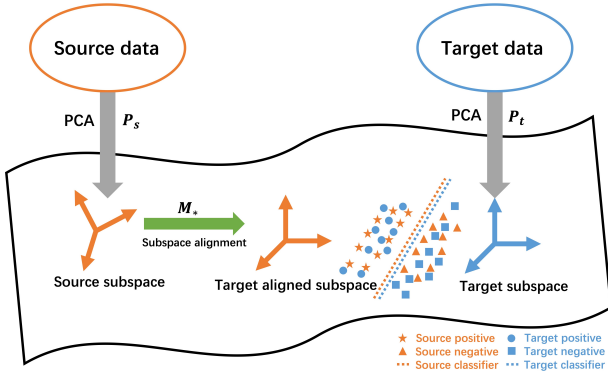


FIG. 1: The illustration of SA.

fore, the whole procedure of the qSA can be implemented with at least quadratic speedup compared to the classical SA.

The contents of this paper will be arranged as follows. The classical SA will be briefly reviewed in section II. Based on the classical SA, the qSA will be presented in section III. Specifically, the source and target domain data is preprocessed by the qPCA to obtain the corresponding subspace data in section III A. Subsequently, the qSA will be implemented in section III B. The target labels will be predicted through the local and global classifiers in section III C. Afterwards, the algorithmic complexity of the classical and quantum SA will be discussed in IV. In addition, the qSA is extended to the quantum kernel subspace alignment algorithm (qKSA) in section V. Finally, we make a conclusion in section VI.

II. CLASSICAL SUBSPACE ALIGNMENT

In the field of transfer learning, domain \mathcal{D} refers to the data set X and its corresponding distribution $P(X)$. Given a labelled source domain $\mathcal{D}_s = \{(x_{s_i}, y_{s_i})\}_{i=1}^{n_s} \in \mathbb{R}^{D \times n_s}$ and an unlabelled target domain $\mathcal{D}_t = \{x_{t_j}\}_{j=1}^{n_t} \in \mathbb{R}^{D \times n_t}$, and the corresponding data distributions $P(X_s) \neq P(X_t)$. DA attempts to obtain the labels of \mathcal{D}_t with utilizing the knowledge of \mathcal{D}_s [2]. After projecting the source domain data set $X_s = \{x_{s_i}\}_{i=1}^{n_s}$ and the target domain data set $X_t = \{x_{t_j}\}_{j=1}^{n_t}$ to their subspaces respectively, the SA aims to align the two subspaces with some linear transformations. So that, the classifier f trained on \mathcal{D}_s can be applied to \mathcal{D}_t to predict the target labels y_t of \mathcal{D}_t [10]. The illustration of classical SA is presented in Fig. 1.

In the first step, with the principal component analysis algorithm (PCA) [46], SA projects X_s and X_t to their corresponding d -dimensional subspaces \hat{X}_s and \hat{X}_t spanned by the columns of P_s and P_t respectively where $d \ll D$ and $P_s, P_t \in \mathbb{R}^{D \times d}$.

Subsequently, the source domain subspace basis can be aligned to the target domain subspace basis with a trans-

formation matrix $M \in \mathbb{R}^{d \times d}$. The objective function is

$$\begin{aligned} M_* &= \arg \min_M \|P_s M - P_t\|_F^2 \\ &= \arg \min_M \|P_s^T P_s M - P_s^T P_t\|_F^2 \\ &= \arg \min_M \|M - P_s^T P_t\|_F^2. \end{aligned} \quad (1)$$

Hence, the optimal transformation matrix $M_* = P_s^T P_t$. The source domain subspace can be aligned to the target domain subspace with $P_a = P_s M_*$. The target aligned source domain subspace data set $\hat{X}_a = \{\hat{x}_{a_i}\}_{i=1}^{n_s} \in \mathbb{R}^{d \times n_s}$ and the target domain subspace data set $\hat{X}_t = \{\hat{x}_{t_j}\}_{j=1}^{n_t} \in \mathbb{R}^{d \times n_t}$ can be obtained as follows

$$\hat{X}_a = P_a^T X_s = (P_s M_*)^T X_s, \quad (2)$$

$$\hat{X}_t = P_t^T X_t. \quad (3)$$

The similarity function which measures the discrepancy between the source and the target domain data set is defined as

$$\begin{aligned} sim(x_s, x_t) &= (\hat{x}_s)^T \hat{x}_t \\ &= x_s^T P_s M_* P_t^T x_t \\ &= x_s^T A x_t \end{aligned} \quad (4)$$

where the target aligned matrix $A = P_s M_* P_t^T$ [10].

After aligning the subspaces, the classifier can be applied to obtain the target data labels y_t . The local classifier such as the nearest-neighbor algorithm can be performed on \hat{X}_a and \hat{X}_t to predict the target labels y_t [47]. In addition, the global classifier such as the support vector machine (SVM) can be trained on \mathcal{D}_s and transferred to \mathcal{D}_t to classify y_t with the matrix A [48].

III. QUANTUM SUBSPACE ALIGNMENT

In this section, the qSA will be presented. At first, the source and target data sets will be preprocessed by the qPCA. Then, the source and target subspace will be aligned. Finally, the quantum classifiers will be applied to obtain the target labels.

A. Data preprocessing

According to section II, X_s and X_t can be preprocessed by the qPCA to obtain the corresponding principle components and subspace data sets [21]. The quantum states corresponding to X_s and X_t are

$$|\psi_{X_s}\rangle = \sum_{i=1}^{n_s} \sum_{m=1}^D x_{mi}^{(s)} |i\rangle |m\rangle, \quad (5)$$

$$|\psi_{X_t}\rangle = \sum_{j=1}^{n_t} \sum_{m=1}^D x_{mj}^{(t)} |j\rangle |m\rangle, \quad (6)$$

respectively. Thus, the quantum state which is proportional to the covariance matrix $C_s = X_s X_s^T$ is

$$\begin{aligned} \rho_{C_s} &= \text{tr}_i \{ |\psi_{X_s}\rangle \langle \psi_{X_s}| \} \\ &= \sum_{m, m'=1}^D \sum_{i=1}^{n_s} x_{mi}^{(s)} x_{m'i}^{(s)*} |m\rangle \langle m'| \end{aligned} \quad (7)$$

where tr_i is the partial trace over the i register.

Apply the controlled swap operation $CU_S = |0\rangle\langle 0| \otimes I + |1\rangle\langle 1| \otimes e^{-iS\Delta t}$ on the states $\sigma \otimes (\rho_{C_s}^{\otimes l})$ repeatedly resulting in

$$CU_{C_s} = \sum_{l=0}^l |l\Delta t\rangle \langle l\Delta t| \otimes e^{-i\rho_{C_s} l\Delta t} |\psi_{X_s}\rangle \langle \psi_{X_s}| e^{i\rho_{C_s} l\Delta t} \quad (8)$$

where the slice time $\Delta t = t/l$ for some large l [21].

Subsequently, the source domain d -dimensional subspace principal components

$$P_s = \sum_{i=1}^d |u_i^{(s)}\rangle \langle u_i^{(s)}| \quad (9)$$

can be obtained by applying the quantum phase estimation

$$\begin{aligned} \mathbf{U}_{\mathbf{PE}}(\rho_{C_s}) &= (\mathbf{QFT}^\dagger \otimes \mathbf{I}) \left(\sum_{\tau=0}^{T-1} |\tau\rangle \langle \tau| \otimes e^{iG\tau t/T} \right) \\ &(\mathbf{H}^{\otimes n} \otimes \mathbf{I}) \end{aligned} \quad (10)$$

on the quantum state ρ_{C_s} and sampling the eigenvectors $|u_i^{(s)}\rangle$ which are corresponding to the d largest eigenvalues of ρ_{C_s} where \mathbf{QFT}^\dagger represents the inverse quantum Fourier transform [21, 49]. Similarly, the target domain d -dimensional subspace data $P_t = \sum_{j=1}^d |u_j^{(t)}\rangle \langle u_j^{(t)}|$ can be obtained with the qPCA.

B. Subspace alignment

As presented in the data preprocessing section, the quantum states representing the source and target principal components are

$$|P_s\rangle = \frac{1}{\|P_s\|_F} \sum_{i=1}^d \sum_{p=1}^d u_{pi}^{(s)} |i\rangle |p\rangle = \frac{1}{\|P_s\|_F} \sum_{i=1}^d |u_{s_i}\rangle |i\rangle |u_{s_i}\rangle, \quad (11)$$

$$|P_t\rangle = \frac{1}{\|P_t\|_F} \sum_{j=1}^d \sum_{p=1}^d u_{pj}^{(t)} |j\rangle |p\rangle = \frac{1}{\|P_t\|_F} \sum_{j=1}^d |u_{t_j}\rangle |j\rangle |u_{t_j}\rangle, \quad (12)$$

respectively where $\|\cdot\|_F$ is the Frobenius norm. Subsequently, the quantum states

$$\begin{aligned} \rho_s &= \text{tr}_i \{ |P_s\rangle \langle P_s| \} \\ &= \sum_{p, p'=1}^d \sum_{i=1}^d u_{pi}^{(s)} u_{pi}^{(s)*} |p\rangle \langle p'| \end{aligned} \quad (13)$$

and

$$\begin{aligned} \rho_t &= \text{tr}_j \{ |P_t\rangle \langle P_t| \} \\ &= \sum_{p, p'=1}^d \sum_{j=1}^d u_{pj}^{(t)} u_{pj}^{(t)*} |p\rangle \langle p'| \end{aligned} \quad (14)$$

which are proportional to $P_s P_s^T$ and $P_t P_t^T$ respectively can be obtained [20].

The preparation procedure of the optimal transformation matrix $M_* = P_s^T P_t$ is presented as follows.

(1) Prepare the initial state. Given the quantum states $|P_s\rangle$ and $|P_t\rangle$, assume that the quantum oracle is accessible

$$\mathbf{U}_S(P) : |i\rangle |0\rangle \rightarrow \frac{1}{\|P\|} |u_i\| |i\rangle |u_i\rangle. \quad (15)$$

The initial state

$$|\psi_0\rangle = \sum_{i, j=1}^d |i\rangle^{I_1} |j\rangle^{I_2} |0\rangle^B |0\rangle^{C_1} \quad (16)$$

can be prepared with four quantum registers.

Apply the Hadamard operation \mathbf{H} and the controlled unitary $\mathbf{U}_P(P_s, P_t) = I^{I_2} \otimes |0\rangle\langle 0|^B \otimes \mathbf{U}_S^{I_1 C_1}(P_s) + I^{I_1} \otimes |1\rangle\langle 1|^B \otimes \mathbf{U}_S^{I_2 C_1}(P_t)$ on the initial state resulting in

$$\begin{aligned} |\psi_1\rangle &= \frac{1}{\sqrt{2}} (|0\rangle |P_s\rangle + |1\rangle |P_t\rangle) \\ &= \frac{1}{\|P_s\|_F \|P_t\|_F} \sum_{i, j=1}^d |u_{s_i}\rangle |u_{t_j}\rangle |i\rangle^{I_1} |j\rangle^{I_2} \otimes |\phi_0\rangle^{BC_1}, \end{aligned} \quad (17)$$

where $|\phi_0\rangle = \frac{1}{\sqrt{2}} (|0\rangle |u_{s_i}\rangle + |1\rangle |u_{t_j}\rangle)$ [50].

(2) The quantum state

$$|\psi_2\rangle = \frac{1}{\|P_s\|_F \|P_t\|_F} \sum_{i, j=1}^d |u_{s_i}\rangle |u_{t_j}\rangle |i\rangle^{I_1} |j\rangle^{I_2} \otimes |\phi_1\rangle^{BC_1} \quad (18)$$

can be obtained with applying the Hadamard operation \mathbf{H} on the $|\phi_0\rangle$ register where $|\phi_1\rangle = \frac{1}{2} (|0\rangle (|u_{s_i}\rangle + |u_{t_j}\rangle) + |1\rangle (|u_{s_i}\rangle - |u_{t_j}\rangle))$.

Let

$$\begin{aligned} |\phi_1\rangle &= \sin \theta_{ij} |0\rangle |u_1\rangle + \cos \theta_{ij} |1\rangle |u_2\rangle \\ &= -\frac{i}{\sqrt{2}} (e^{i\theta_{ij}} |w_1\rangle - e^{-i\theta_{ij}} |w_2\rangle) \end{aligned} \quad (19)$$

where $\sin \theta_{ij} = \frac{\sqrt{(1 + \langle u_{s_i} | u_{t_j} \rangle)}}{2}$, $\cos \theta_{ij} = \frac{\sqrt{(1 - \langle u_{s_i} | u_{t_j} \rangle)}}{2}$, and $|u_1\rangle$, $|u_2\rangle$ represent the normalization of $|u_{s_i}\rangle + |u_{t_j}\rangle$, $|u_{s_i}\rangle - |u_{t_j}\rangle$ respectively. In addition, the quantum states

$$\begin{cases} |w_1\rangle = \frac{1}{\sqrt{2}} (|0\rangle |u_1\rangle + i |1\rangle |u_2\rangle), \\ |w_2\rangle = \frac{1}{\sqrt{2}} (|0\rangle |u_1\rangle - i |1\rangle |u_2\rangle); \end{cases} \quad (20)$$

are the eigenvectors of the matrix $G = (2|\phi_1\rangle\langle\phi_1| - I)(-\sigma_z \otimes I)$ corresponding to the eigenvalues $e^{\pm i2\theta_{ij}}$ where σ_z is the Pauli-Z operator [45].

(3) The quantum phase estimation $\mathbf{U}_{\text{PE}}(G)$ is applied on the quantum state $|\phi_1\rangle$ register resulting in

$$|\psi_3\rangle = -\frac{i}{\sqrt{2}\|P_s\|_F\|P_t\|_F} \sum_{i,j=1}^d |u_{s_i}\|u_{t_j}\|i\rangle^{I_1}|j\rangle^{I_2} \otimes (e^{i\theta_{ij}}|w_1\rangle^{BC_1}|\tilde{\lambda}\rangle^{C_2} - e^{-i\theta_{ij}}|w_2\rangle^{BC_1}|\tilde{\lambda}\rangle^{C_2}), \quad (21)$$

where $\theta_{ij} = \tilde{\lambda}\pi/2^n$ [49].

(4) Add a new register R and perform the conditional rotation \mathbf{U}_{CR} on it to obtain the state

$$|\psi_4\rangle = |\psi_3\rangle \otimes (\langle u_{s_i}|u_{t_j}\rangle|0\rangle^R + \sqrt{1 - \langle u_{s_i}|u_{t_j}\rangle^2}|1\rangle^R). \quad (22)$$

(5) We uncompute the $|w\rangle$ and $|\lambda\rangle$ registers and measure the R register to be $|0\rangle$. The final state

$$|\psi_{M_*}\rangle = \frac{1}{\|P_s\|_F\|P_t\|_F} \sum_{i,j=1}^d |u_{s_i}\|u_{t_j}\langle u_{s_i}|u_{t_j}\rangle|i\rangle|j\rangle \quad (23)$$

can be obtained which represents the matrix $M_* = P_s^T P_t$.

For simplicity, the procedure of matrix multiplication above can be represented as the unitary evolution

$$\mathbf{U}_{\text{M}}(P_s, P_t) = \mathbf{U}_1^\dagger \mathbf{U}_2^\dagger \mathbf{U}_3^\dagger \mathbf{U}_4 \mathbf{U}_3 \mathbf{U}_2 \mathbf{U}_1. \quad (24)$$

where

$$\begin{cases} \mathbf{U}_1 = \mathbf{U}_{\text{P}}(P_s, P_t)(\mathbf{I}^{I_1 I_2 C_1} \otimes \mathbf{H}^B), \\ \mathbf{U}_2 = \mathbf{I}^{I_1 I_2 C_1} \otimes \mathbf{H}^B, \\ \mathbf{U}_3 = \mathbf{I}^{I_1 I_2} \otimes \mathbf{U}_{\text{PE}}^{BC_1 C_2}(G), \\ \mathbf{U}_4 = \mathbf{I}^{I_1 I_2 BC_1} \otimes \mathbf{U}_{\text{CR}}^{C_2 R}. \end{cases} \quad (25)$$

Hence, the quantum state

$$|\psi_{\hat{X}_s}\rangle = \mathbf{U}_{\text{M}}(P_s, X_s)|\psi_0\rangle = \frac{1}{\|\hat{X}_s\|_F} \sum_{i=1}^{n_s} \sum_{m=1}^d \hat{x}_{mi}^{(s)}|i\rangle|m\rangle \quad (26)$$

which contains the elements of the source domain subspace data set \hat{X}_s . With the quantum states $|\psi_{M_*}\rangle$ and $|\psi_{\hat{X}_s}\rangle$, the unitary operation $\mathbf{U}_{\text{M}}(M_*, \hat{X}_s)$ can be applied on $|\psi_0\rangle$ resulting in the quantum target aligned source subspace state

$$|\psi_{\hat{X}_a}\rangle = \mathbf{U}_{\text{M}}(M_*, \hat{X}_s)|\psi_0\rangle = \frac{1}{\|\hat{X}_a\|_F} \sum_{i=1}^{n_s} |i\rangle|\hat{x}_{ia}\rangle. \quad (27)$$

Similarly, the quantum state corresponding to the target subspace data set \hat{X}_t is

$$|\psi_{\hat{X}_t}\rangle = \mathbf{U}_{\text{M}}(P_t, X_t)|\psi_0\rangle = \frac{1}{\|\hat{X}_t\|_F} \sum_{i=1}^{n_t} \sum_{m=1}^d \hat{x}_{mi}^{(t)}|i\rangle|m\rangle. \quad (28)$$

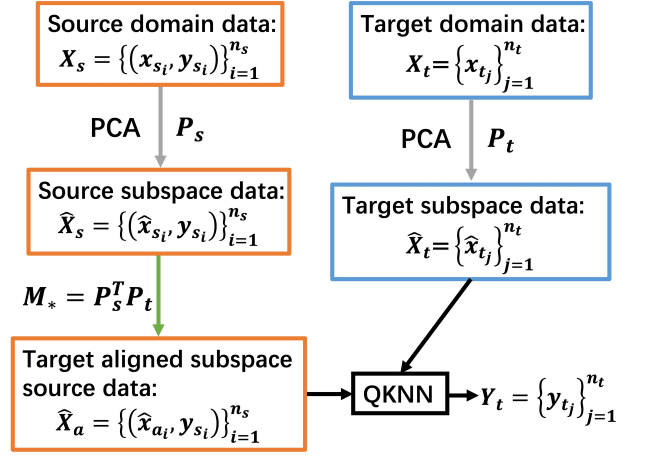


FIG. 2: The schematic diagram of the qSA algorithm with quantum nearest-neighbor algorithm.

In addition, the target aligned matrix A can be represented by the quantum state

$$|\psi_A\rangle = \mathbf{U}_{\text{M}}(\rho_s, \rho_t)|\psi_0\rangle. \quad (29)$$

Ultimately, the D -dimensional source domain data set X_s is projected to the d -dimensional source domain subspace data set \hat{X}_s and subsequently aligned to the target aligned source subspace data set \hat{X}_a . And the target domain data set X_t is projected to the target domain subspace data set \hat{X}_t . In the following, two different quantum classifiers will be applied to predict the target labels y_t .

C. Classification

After obtaining \hat{X}_a and \hat{X}_t , the quantum nearest-neighbor algorithm, a quantum local classifier can be applied on them to find y_t [24, 25]. In addition, with X_s , X_t and A , the qSVM, a global classifier can also be utilized to predict the labels of the target domain data [23].

1. Local classifier

The local classifier is a kind of algorithm utilizing the local information around the target domain subspace data point \hat{x}_{t_j} to classify the corresponding label y_{t_j} . The quantum nearest-neighbor algorithm is a representative local classification algorithm [24, 25]. It can be applied on \hat{X}_a and \hat{X}_t to obtain y_t . In the following, the concrete procedure of the classification will be presented. The procedure of applying the quantum nearest-neighbor algorithm is depicted in Fig. 2.

As in ref. [25], the target subspace data \hat{x}_{t_j} which re-

mains to be classified can be stored in the quantum state

$$|\alpha\rangle = \frac{1}{\sqrt{d}} \sum_{p=1}^d |p\rangle (\sqrt{1 - \hat{x}_{pj}^{(t)2}} |0\rangle + \hat{x}_{pj}^{(t)} |1\rangle) |0\rangle. \quad (30)$$

And the training set, namely the target aligned source subspace data set \hat{X}_a , can be stored in the quantum state

$$|\beta\rangle = \frac{1}{\sqrt{n_s}} \sum_{i=1}^{n_s} |i\rangle \frac{1}{\sqrt{d}} |p\rangle |0\rangle (\sqrt{1 - \hat{x}_{pi}^{(a)2}} |0\rangle + \hat{x}_{pi}^{(a)} |1\rangle). \quad (31)$$

Subsequently, the swap test [51] can be performed on the quantum state $|0\rangle|\alpha\rangle|\beta\rangle$ resulting in

$$|\gamma\rangle = \frac{1}{\sqrt{n_s}} \sum_{i=1}^{n_s} |i\rangle (\sqrt{1 - |\hat{x}_{t_j} - \hat{x}_{a_i}|} |0\rangle + \sqrt{|\hat{x}_{t_j} - \hat{x}_{a_i}|} |1\rangle). \quad (32)$$

With the amplitude estimation algorithm [52], the distance between \hat{x}_{t_j} and \hat{x}_{a_i} can be encoded in the ancilla register

$$|\sigma\rangle = \frac{1}{n_s} \sum_{i=1}^{n_s} |i\rangle |\hat{x}_{t_j} - \hat{x}_{a_i}\rangle. \quad (33)$$

Finally, the training set data point $\hat{x}_{a_{min}}$ which is closest to \hat{x}_{t_j} can be found out by applying the Dürr's algorithm on the quantum state $|\sigma\rangle$ in $O(\sqrt{n_s})$ [53]. Hence, the target label y_{t_j} of the target domain data x_{t_j} can be classified to the same class as $\hat{x}_{a_{min}}$.

2. Global classifier

The global classifier utilizes the global information of the data set to classify the target data labels. The qSVM is an efficient global classification algorithm [23]. The whole procedure mainly contains two parts: the training and the classification.

In the training section, the SVM parameters can be obtained with the source domain data $\mathcal{D}_s = \{(x_{s_i}, y_{s_i})\}_{i=1}^{n_s}$ used as the training set and the training kernel matrix $K_{s,s} = \text{sim}(X_s, X_s)$. Refer to ref. [23], the SVM parameters

$$\begin{pmatrix} b \\ \alpha \end{pmatrix} = \begin{pmatrix} 0 & \mathbf{1}^T \\ \mathbf{1} & K_{s,s} + \gamma^{-1}I \end{pmatrix}^{-1} \begin{pmatrix} 0 \\ y_s \end{pmatrix}, \quad (34)$$

where $y_s = (y_{s_1}, y_{s_2}, \dots, y_{s_{n_s}})^T$, $\mathbf{1} = (1, 1, \dots, 1)^T$ and γ_1 is a constant.

Let

$$F_s = \begin{pmatrix} 0 & \mathbf{1}^T \\ \mathbf{1} & K_{s,s} + \gamma_1^{-1}I \end{pmatrix} \quad (35)$$

where its normalization $\hat{F}_s = \frac{F_s}{\text{tr}(F_s)}$, the matrix

$$J = \begin{pmatrix} 0 & \mathbf{1}^T \\ \mathbf{1} & 0 \end{pmatrix} \quad (36)$$

and the matrix

$$K_\gamma = \begin{pmatrix} 0 & 0 \\ 0 & K_{s,s} + \gamma_1^{-1}I \end{pmatrix}. \quad (37)$$

The SVM parameters $|b, \alpha\rangle = \hat{F}_s^{-1}|y\rangle$ can be obtained by applying the quantum matrix inversion algorithm where $|y\rangle = \frac{1}{|y_s|} (0, y_s)^T$ [17].

In the classification section, we substitute the SVM parameters $|b, \alpha\rangle$ into the SVM model to classify the target labels y_t as presented in [23]. With the target domain data $\mathcal{D}_t = \{x_{t_j}\}_{j=1}^{n_t}$ and the target aligned matrix A , the query state

$$|\psi_{x_{t_j}}\rangle = \frac{1}{\sqrt{N_t}} (|0\rangle|0\rangle + \sum_{i=1}^{n_s} |x_{t_j}|A|i\rangle|x_{t_j}\rangle) \quad (38)$$

can be constructed where $N_t = n_s|x_{t_j}|^2 + 1$ is the norm of $|\psi_{x_{t_j}}\rangle$. And the training data can be encoded to the quantum state

$$|\psi_t\rangle = \frac{1}{\sqrt{N_x}} (b|0\rangle|0\rangle + \sum_{i=1}^{n_s} \alpha_{i=1} |x_{s_i}| |i\rangle |x_{s_i}\rangle) \quad (39)$$

through the quantum oracles where $N_x = b^2 + \sum_{i=1}^{n_s} \alpha_i^2 |x_{s_i}|^2$ is the norm of $|\psi_t\rangle$.

Subsequently, the inner product of $|\psi_{x_{t_j}}\rangle$ and $|\psi_t\rangle$ can be computed as

$$\begin{aligned} \langle \psi_t | \psi_{x_{t_j}} \rangle &= \frac{1}{\sqrt{N_x N_t}} (b + \sum_{i=1}^{n_s} \alpha_i |x_{s_i}| |x_{t_j}| \langle x_{s_i} | A | x_{t_j} \rangle) \\ &= \frac{1}{\sqrt{N_x N_t}} (b + \sum_{i=1}^{n_s} \alpha_i K_{s_i, t_j}). \end{aligned} \quad (40)$$

Therefore, the label of the target domain data point x_{t_j}

$$y_{t_j} = \text{sign} \left(\sum_{i=1}^{n_s} \alpha_i K_{s_i, t_j} + b \right) \quad (41)$$

can be obtained. The whole process above is presented in Fig. 3.

IV. ALGORITHMIC COMPLEXITY

To evaluate the performance of the classical and quantum SA algorithm, the algorithmic complexity of the two algorithms will be analyzed in this section.

The classical SA algorithm mainly contains three parts. In the data preprocessing, the classical SA algorithm utilizes the PCA to project the source and target domain data sets to the corresponding d -dimensional subspace in $O((n_s + n_t)D + D^3)$ [46]. The procedure of aligning the subspaces can be implemented in $O(D^2d)$ [10]. As to the classification after the subspace alignment, two different types of classifiers can be applied. For the local classifier, the nearest-neighbor algorithm can be performed on the target aligned source subspace data set

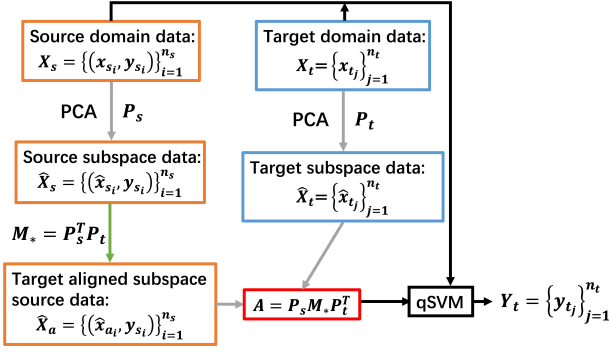


FIG. 3: The schematic diagram of the qSA algorithm with quantum nearest-neighbor algorithm.

\hat{X}_a and the target subspace data set \hat{X}_t to classify the target labels y_t in $O(n_s \log n_s)$ [47]. For the global classifier, the SVM can be implemented with polynomial time complexity in the number of training samples n_s and the original data dimension D [48].

Compared with the classical SA, the source and target domain data sets are preprocessed by the qPCA in $O(d \log D)$ [21]. Subsequently, the source domain subspace data \hat{X}_s can be aligned to the target domain subspace data \hat{X}_t with quadratic speedup in $O(\text{poly}(\sqrt{D}/\epsilon))$ where ϵ is the accuracy parameter [45]. Afterwards, we adopt two kinds of quantum classifiers to predict target labels referring to the corresponding classical algorithms. The quantum nearest-neighbor algorithm can be implemented in $O(\text{poly}(\sqrt{n_s}))$ [24, 25]. And the qSVM classifies the target labels in $O(\log(Dn_s))$ [23]. The quantum nearest-neighbor algorithm can directly classify the target labels quadratically faster without training and the qSVM can achieve exponential speedup compared to the corresponding classical algorithms. Therefore, the procedure of DA can be implemented by the qSA presented in this paper with at least quadratic speedup.

V. QUANTUM KERNEL SUBSPACE ALIGNMENT

Although SA is efficient in domain adaptation, the nonlinear characteristics of the given data may not be fully reflected in some cases probably weakening the transfer learning performance. Inspired by the kernel SA algorithm [54], the qKSA will be presented in this section.

The core of the kernel method is to select a feature map

$$\phi : x \rightarrow |\phi(x)\rangle \quad (42)$$

to construct the kernel function

$$K(x_i, x_j) = \langle \phi(x_i) | \phi(x_j) \rangle. \quad (43)$$

The kernel function $K(x_i, x_j)$ has many choices such as

$$\begin{cases} \text{linear kernel : } K_l(x_i, x_j) = \langle x_i | x_j \rangle; \\ \text{polynomial kernel : } K_p(x_i, x_j) = \langle x_i | x_j \rangle^n; \\ \text{cosine kernel : } K_c(x_i, x_j) = \prod_{m=1}^D \cos(x_{mi} - x_{mj}); \\ \text{hard kernel : } K_h(x_i, x_j) = \langle 0 |^{\otimes q} \mathbf{U}_\phi^\dagger(x_i) \mathbf{U}_\phi(x_j) | 0 \rangle^{\otimes q}; \end{cases} \quad (44)$$

where $q = \log D$, n is a constant and $\mathbf{U}_\phi(x)$ can be implemented by variational quantum circuits [55, 56].

The kernel source domain data set

$$\phi(X_s) = |\phi(x_{s_i})\rangle \sum_{i=1}^{n_s} |\phi(x_{s_i})\rangle \langle i| \quad (45)$$

and the kernel target domain data set

$$\phi(X_t) = |\phi(x_{t_j})\rangle \sum_{j=1}^{n_t} |\phi(x_{t_j})\rangle \langle j|. \quad (46)$$

With the PCA, the kernel source subspace data set \hat{X}_s and the kernel target subspace data set $X \hat{X}_t$ can be spanned by the columns of $P_s^\phi = \phi(X_s)W_s$ and $P_t^\phi = \phi(X_t)W_t$ respectively where W_s, W_t are $n_s \times d, n_t \times d$ matrices respectively [57].

The objective function

$$\begin{aligned} M_*^\phi &= \arg \min_M \|P_s^\phi M - P_t^\phi\|_F^2 \\ &= \arg \min_M \|\phi(X_s)W_s M - \phi(X_t)W_t\|_F^2. \end{aligned} \quad (47)$$

Hence, the optimal kernel transformation matrix

$$\begin{aligned} M_*^\phi &= (\phi(X_s)W_s)^T \phi(X_t)W_t \\ &= W_s^T K_{st} W_t \end{aligned} \quad (48)$$

where

$$\begin{aligned} K_{st} &= \phi(X_s)^T \phi(X_t) \\ &= \sum_{i=1}^{n_s} \sum_{j=1}^{n_t} |\phi(x_{s_i})\rangle \langle \phi(x_{t_j})| \langle \phi(x_{s_i}) | \phi(x_{t_j}) \rangle |i\rangle \langle j| \end{aligned} \quad (49)$$

is the corresponding kernel matrix. The d -dimensional kernel target aligned source subspace data $\phi(\hat{X}_a) = (P_s^\phi M_*^\phi \phi(X_s))$ and the target subspace data $\phi(\hat{X}_t) = P_t^{\phi T} \phi(X_t)$ [54]. In addition, the kernel target aligned matrix $A^\phi = P_s^\phi M_*^\phi P_t^{\phi T}$ and the kernel similarity function

$$\begin{aligned} \text{sim}^\phi(\phi(x_s), \phi(x_t)) &= \langle \phi(\hat{x}_s) | \phi(\hat{x}_t) \rangle \\ &= \langle \phi(x_s) | A^\phi | \phi(x_t) \rangle. \end{aligned} \quad (50)$$

After the procedure of the qKSA, the classifiers can be utilized to predict the target labels. Similar to the qSA, the classification can also be implemented with the local and the global classifiers. For the local classifier, the quantum nearest-neighbor algorithm can be performed on $\phi(\hat{X}_a)$ and $\phi(\hat{X}_t)$ to obtain the target labels y_t . For the global classifier, the qSVM can classify y_t with $\phi(X_s), \phi(X_t)$ and $\text{sim}^\phi(\phi(x_s), \phi(x_t))$.

VI. CONCLUSION

In this paper, we have presented an implement of a representative domain adaptation algorithm, SA, on a quantum computer. In the data preprocessing, we perform the qPCA algorithm on the given raw data sets to obtain the subspace data sets with complexity logarithmic in the numbers of the data points [21]. Subsequently, the labelled subspace data set is aligned with the target unlabelled subspace data based on the quantum matrix multiplication operations [45]. The procedure of subspace alignment is implemented on a quantum computer with quadratic speedup. Finally, the local classifier, the quantum nearest-neighbor algorithm and the global classifier, the qSVM, are performed respectively. The quantum nearest neighbor algorithm is applied to the target aligned data and the target data point to obtain the corresponding target label in $O(\text{poly}(\sqrt{n_s}))$ without the

training procedure [24, 25]. In addition, the raw labelled data set and the similarity function can be utilized to train a qSVM model and the label of the target data point can be classified with input the target data and the matrix A achieving exponential speedup [23]. Over the whole procedure, the quantum SA algorithm proposed in our work achieves at least quadratic speedup with algorithmic complexity compared with the classical SA algorithm. The quantum circuit depth of the quantum SA algorithm can be relative high in practice. However, the quantum SA algorithm in our work proves that quantum computation techniques can be applied to the field of transfer learning to accomplish machine learning tasks.

ACKNOWLEDGMENTS

This work is supported by the National Key R&D Program of China, Grant No. 2018YFA0306703.

-
- [1] L. Y. Pratt, in *Advances in neural information processing systems* (1993) pp. 204–211.
 - [2] S. J. Pan and Q. Yang, *IEEE Transactions on knowledge and data engineering* **22**, 1345 (2009).
 - [3] B. Kulis, K. Saenko, and T. Darrell, in *CVPR 2011* (IEEE, 2011) pp. 1785–1792.
 - [4] L. Duan, I. W. Tsang, D. Xu, and S. J. Maybank, in *2009 IEEE Conference on Computer Vision and Pattern Recognition* (IEEE, 2009) pp. 1375–1381.
 - [5] K. Saenko, B. Kulis, M. Fritz, and T. Darrell, in *European conference on computer vision* (Springer, 2010) pp. 213–226.
 - [6] H. Daume III and D. Marcu, *Journal of artificial Intelligence research* **26**, 101 (2006).
 - [7] B. Gong, K. Grauman, and F. Sha, in *International Conference on Machine Learning* (2013) pp. 222–230.
 - [8] J. Ni, Q. Qiu, and R. Chellappa, in *Proceedings of the IEEE conference on computer vision and pattern recognition* (2013) pp. 692–699.
 - [9] A. Shrivastava, S. Shekhar, and V. M. Patel, in *IEEE Winter conference on Applications of Computer Vision* (IEEE, 2014) pp. 277–284.
 - [10] B. Fernando, A. Habrard, M. Sebban, and T. Tuytelaars, in *Proceedings of the IEEE international conference on computer vision* (2013) pp. 2960–2967.
 - [11] B. Sun and K. Saenko, in *BMVC*, Vol. 4 (2015) pp. 24–1.
 - [12] B. Sun and K. Saenko, in *European Conference on Computer Vision* (Springer, 2016) pp. 443–450.
 - [13] R. Gopalan, R. Li, and R. Chellappa, in *2011 international conference on computer vision* (IEEE, 2011) pp. 999–1006.
 - [14] B. Gong, Y. Shi, F. Sha, and K. Grauman, in *2012 IEEE Conference on Computer Vision and Pattern Recognition* (IEEE, 2012) pp. 2066–2073.
 - [15] P. W. Shor, in *Proceedings 35th annual symposium on foundations of computer science* (Ieee, 1994) pp. 124–134.
 - [16] L. K. Grover, arXiv preprint quant-ph/9605043 (1996).
 - [17] A. W. Harrow, A. Hassidim, and S. Lloyd, *Physical review letters* **103**, 150502 (2009).
 - [18] S. Aaronson and A. Arkhipov, in *Proceedings of the forty-third annual ACM symposium on Theory of computing* (ACM, 2011) pp. 333–342.
 - [19] E. Farhi and H. Neven, arXiv preprint arXiv:1802.06002 (2018).
 - [20] S. Lloyd, M. Mohseni, and P. Rebentrost, arXiv preprint arXiv:1307.0411 (2013).
 - [21] S. Lloyd, M. Mohseni, and P. Rebentrost, *Nature Physics* **10**, 631 (2014).
 - [22] P. Rebentrost, A. Steffens, and S. Lloyd, arXiv preprint arXiv:1607.05404 (2016).
 - [23] P. Rebentrost, M. Mohseni, and S. Lloyd, *Physical review letters* **113**, 130503 (2014).
 - [24] N. Wiebe, A. Kapoor, and K. M. Svore, *Quantum Information and Computation* **15** (2018).
 - [25] Y. Dang, N. Jiang, H. Hu, Z. Ji, and W. Zhang, *Quantum Information Processing* **17**, 239 (2018).
 - [26] N. Wiebe, D. Braun, and S. Lloyd, *Physical review letters* **109**, 050505 (2012).
 - [27] M. Schuld, I. Sinayskiy, and F. Petruccione, *Physical Review A* **94**, 022342 (2016).
 - [28] E. Aïmeur, G. Brassard, and S. Gambs, *Machine Learning* **90**, 261 (2013).
 - [29] I. Cong and L. Duan, *New Journal of Physics* **18**, 073011 (2016).
 - [30] X. He, L. Sun, C. Lyu, and X. Wang, arXiv preprint arXiv:1910.07854 (2019).
 - [31] K. H. Wan, O. Dahlsten, H. Kristjánsson, R. Gardner, and M. Kim, *npj Quantum Information* **3**, 36 (2017).
 - [32] J. Romero, J. P. Olson, and A. Aspuru-Guzik, *Quantum Science and Technology* **2**, 045001 (2017).
 - [33] L. Lamata, U. Alvarez-Rodriguez, J. D. Martín-Guerrero, M. Sanz, and E. Solano, *Quantum Science and Technology* **4**, 014007 (2018).

- [34] A. Khoshaman, W. Vinci, B. Denis, E. Andriyash, and M. H. Amin, *Quantum Science and Technology* **4**, 014001 (2018).
- [35] N. Wiebe, A. Kapoor, and K. M. Svore, arXiv preprint arXiv:1412.3489 (2014).
- [36] M. H. Amin, E. Andriyash, J. Rolfe, B. Kulchytskyy, and R. Melko, *Physical Review X* **8**, 021050 (2018).
- [37] S. Lloyd and C. Weedbrook, *Physical review letters* **121**, 040502 (2018).
- [38] P.-L. Dallaire-Demers and N. Killoran, *Physical Review A* **98**, 012324 (2018).
- [39] L. Hu, S.-H. Wu, W. Cai, Y. Ma, X. Mu, Y. Xu, H. Wang, Y. Song, D.-L. Deng, C.-L. Zou, *et al.*, *Science advances* **5**, eaav2761 (2019).
- [40] M. Benedetti, E. Grant, L. Wossnig, and S. Severini, *New Journal of Physics* **21**, 043023 (2019).
- [41] H. Situ, Z. He, L. Li, and S. Zheng, arXiv preprint arXiv:1807.01235 (2018).
- [42] J. Zeng, Y. Wu, J.-G. Liu, L. Wang, and J. Hu, *Physical Review A* **99**, 052306 (2019).
- [43] A. Mari, T. R. Bromley, J. Izaac, M. Schuld, and N. Killoran, arXiv preprint arXiv:1912.08278 (2019).
- [44] X. He, C. Lyu, M.-H. Hsieh, and X. Wang, arXiv preprint arXiv:1912.09113 (2019).
- [45] C. Shao, arXiv preprint arXiv:1803.01601 (2018).
- [46] K. Pearson, *The London, Edinburgh, and Dublin Philosophical Magazine and Journal of Science* **2**, 559 (1901).
- [47] G. Gutin, A. Yeo, and A. Zverovich, *Discrete Applied Mathematics* **117**, 81 (2002).
- [48] C. Cortes and V. Vapnik, *Machine learning* **20**, 273 (1995).
- [49] M. A. Nielsen and I. Chuang, *Quantum computation and quantum information* (2002).
- [50] K. Zhang, M.-H. Hsieh, L. Liu, and D. Tao, arXiv preprint arXiv:1909.07622 (2019).
- [51] H. Buhrman, R. Cleve, J. Watrous, and R. De Wolf, *Physical Review Letters* **87**, 167902 (2001).
- [52] G. Brassard, P. Hoyer, M. Mosca, and A. Tapp, *Contemporary Mathematics* **305**, 53 (2002).
- [53] C. Durr and P. Hoyer, arXiv preprint quant-ph/9607014 (1996).
- [54] M. Xu, S. Wu, X.-Y. Jing, and J. Yang, in *2015 IEEE International Conference on Image Processing (ICIP)* (IEEE, 2015) pp. 2880–2884.
- [55] M. Schuld and N. Killoran, arXiv preprint arXiv:1803.07128 (2018).
- [56] V. Havlíček, A. D. Córcoles, K. Temme, A. W. Harrow, A. Kandala, J. M. Chow, and J. M. Gambetta, *Nature* **567**, 209 (2019).
- [57] B. Schölkopf, A. Smola, and K.-R. Müller, *Neural computation* **10**, 1299 (1998).